EPJ manuscript No.
(will be inserted by the editor)

Future of low-x forward physics at RHIC

L.C. Bland[1], F. Bieser[2], R.L. Brown[1], H.J. Crawford[2], A.A. Derevshchikov[4], J.L. Drachenberg[5], J. Engelage[2], L. Eun[3], C.A. Gagliardi[5], S. Heppelmann[3], E.G. Judd[2], V.I. Kravtsov[4], Yu.A. Matulenko[4], A.P. Meschanin[4], D.A. Morozov[4], L.V. Nogach[4], S.B. Nurushev[4], A. Ogawa[1], C. Perkins[2], G. Rakness[1,3], K.E. Shestermanov[4], and A.N. Vasiliev[4]

[1] Brookhaven National Laboratory
[2] University of Berkeley/Space Sciences Institute
[3] Pennsylvania State University
[4] IHEP, Protvino
[5] Texas A&M University

Received: date / Revised version: date

Abstract. Comparisons of particle production from high-energy ion collisions with next-to-leading order perturbative QCD calculations show good agreement down to moderate transverse momentum values. Distributions of azimuthal angle differences between coincident hadrons in these collisions support a partonic origin to the particle production, again down to moderate transverse momentum values. The rapidity dependence of inclusive and coincident particle production can therefore be used to probe parton distribution functions down to small momentum fractions where theory anticipates that parton saturation could be present. This paper describes how such experiments could be completed.

PACS. 12.38 Qk – 13.88.+e – 24.85.+p

1 Introduction

Comprehensive measurements of p+p, d+Au and Au+Au interactions at $\sqrt{s_{NN}}$=200 GeV by the RHIC experiments strongly suggest that the central collisions of two gold nuclei lead to a new form of matter that appears opaque to high transverse momentum (p_T) hadrons [1]. This dense matter evolves from an initial state produced by the collisions of the low-x gluon fields of each nucleus [2]. Understanding this initial state is the first topic mentioned in a recent report on scientific opportunities in heavy-ion physics. "Upgraded forward instrumentation" was identified as needed to elucidate the properties of the initial state [3]. Nucleon gluon density distributions are determined by global fits to data [4,5], but the low-x nuclear gluon distribution is not yet known [6,7]. The nuclear gluon field distribution might be naively expected to result from a convolution of the gluon density distributions of all the individual nucleons. However, there is indirect experimental evidence from RHIC [8] that the low-x gluon distribution in a large nucleus like gold is reduced, or shadowed, from the nominal superposition of the distributions of the included protons and neutrons, a phenomenon described as saturation. In this document we describe a possible measurement of the gluon distribution in a large nucleus.

In the early runs at RHIC, we have demonstrated that forward electromagnetic calorimeters (Fig. 1), the Forward π^0 Detector (FPD), can be used to measure π^0 produced at large pseudorapidity ($\eta = -\ln\tan\theta/2$, where θ is the polar angle of the produced particle) in p+p and d+Au collisions at $\sqrt{s_{NN}}$=200 GeV at STAR [10]. We have recently proposed to assemble a Forward Meson Spectrometer (FMS) that will be operated during future RHIC running periods by the STAR collaboration to enable measurement of the gluon distribution, $xg(x)$, in nuclei in the range $0.001 < x < 0.1$. The function $g(x)$ gives the differential probability to find gluons with a fraction x of the longitudinal momentum of the parent nucleon (Fig. 2). The FMS will cover the range $2.5 < \eta < 4.0$ and give STAR nearly hermetic electromagnetic coverage

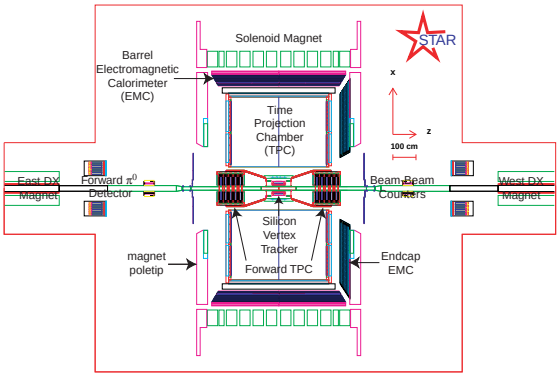

Fig. 1. Layout of the Solenoidal Tracker at RHIC [9]

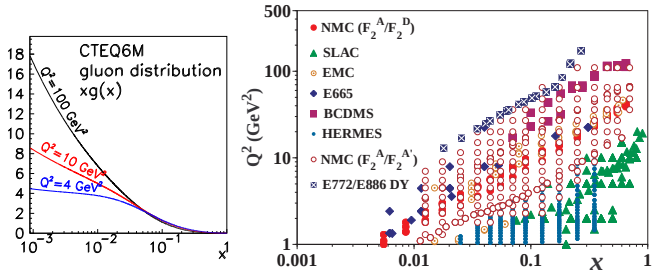

Fig. 2. (Left) The gluon distribution in the proton [4]. Note the rapid rise in $xg(x)$ for $x < 0.01$, a discovery made at HERA based on studies of deep inelastic scattering (DIS), using electron(positron)+proton collisions at $\sqrt{s}$=300 GeV [11, 12]. (Right) Values of DIS kinematic variables x and Q^2 where nuclear data from fixed-target DIS experiments at much lower $\sqrt{s}$ constrain the nuclear gluon density for $x > 0.02$ [6,7].

in the range $-1 < \eta < 4$. The FMS will allow correlation measurements between forward mesons and photons with signals from the full STAR detector, including the barrel and endcap electomagnetic calorimeters (BEMC,EEMC) and the forward and midrapidity time-projection chambers (TPC). Exploiting the capabilities of RHIC and the existing STAR detector, and assuming simple 2-body kinematics, the FMS will allow measurement of the gluon density in protons and in nuclei down to $x \sim 0.001$.

With the addition of the FMS, which has > 25 times larger areal coverage than the FPD we view as its prototype, STAR will be able to achieve at least three important and new physics objectives:

- A measurement of the gluon density distributions in gold nuclei for $0.001 < x < 0.1$, thereby extending our current knowledge and including an overlap region that tests the universality of the gluon distribution.
- Characterization of correlated pion cross sections as a function of p_T to search for the onset of gluon saturation effects associated with macroscopic gluon fields.
- Measurements with transversely polarized protons that are expected to resolve the origin of the large transverse spin asymmetries in $p_\uparrow + p \to \pi^0 + X$ reactions for forward π^0 production.

In d+Au collisions, the FMS will face the deuteron beam and will see neutral pions produced by large-x quarks in the deuteron interacting with the low-x gluons in the Au nucleus. The key to this analysis is the detection of a second particle in coincidence with a triggering particle in the FMS. The coincident signal might be a high-p_T track or jet detected in the TPCs or it might be a γ or π^0 detected in the BEMC or EEMC. For $x < 0.01$, the coincident particle will be a second γ/π^0 detected in the FMS, whose large acceptance makes this coincidence measurement possible. The spatial dependence of the nuclear gluon density [13, 14] will be investigated by analyzing two-particle correlations as a function of particle multiplicity in the Au beam direction with the existing STAR subsystems.

Analysis of the kinematics of the relative momentum between the trigger particle and the coincident particle allows us to determine $g(x)$ in the gold nucleus under the simple assumption of elastic scattering of collinear initial-state partons. This measurement of the gluon density provides the essential input to the simulation codes that attempt to determine the energy density achieved when heavy nuclei collide, in the state which could expand to become the quark gluon plasma.

The same correlated particle analysis will allow us to study the physics of the parton saturation region, if it exists for $Q^2 < 4$ GeV^2. This physics is associated with the transformation from a parton-dominated picture of the nuclear gluon distribution to a picture for which macroscopic QCD fields might play a role or provide the most approporiate physics description. The FMS granularity will enable measurement of the azimuthal angle (ϕ) of the trigger pion and a coincident pion. The peak in the $\Delta\phi = \phi_{\pi 1} - \phi_{\pi 2}$ distribution at 180°, the classic signature of parton elastic scattering, is expected to broaden [15] or disappear [16] (*ie.*, the forward jet becomes a monojet and the recoil hadron rapidity distribution is modified) when scattering from macroscopic gluon fields dominates scattering from single gluons.

The analysis of FMS-triggered events at STAR will also be used in polarized proton running where the extended calorimetry acceptance will greatly enhance our ability to determine how quark and gluon fields conspire to share the proton's $\frac{1}{2}$ unit of spin. Polarized deep inelastic scattering (DIS) experiments found that the intrinsic spin of quarks and antiquarks contribute only $\sim$ 20% to the nucleon spin, contrary to early theoretical expectations of > 60%. A prime objective of the RHIC spin program is to understand how gluon spin and parton orbital angular momentum play a role in this "missing spin puzzle". The correlated pion analysis of the FMS and the analysis channels it opens will play a crucial role in answering these questions and could lead to resolution of the long-standing question about the origin of the large transverse single spin asymmetry in forward pion production.

2 Nuclear gluon densities

A central objective in high energy physics has been the systematic characterization of parton (quark and gluon) density distributions [4,5]. As a consequence of factorization theorems we know that there is a class of high-p_T two-parton (leading twist) experiments that can be understood in terms of an initial state of independent partons within a proton. Within this framework, the part of the cross section due to a particular sub-process is equal to the product of a calculable parton-level cross section and the two universal initial state parton probability densities

$$\sigma(x_n, x_m) \propto \sigma_{nm} f_n(x_n) f_m(x_m).$$

The parton densities $f(x)$ are universal properties of the proton, applicable in all hard scattering processes, and in most cases (but not all) refer to the positive definite probability density to find a parton "n" ($n = q$ for quark, $\overline{q}$ for antiquark and g for gluon, with $f_g(x)$ referred to as

$g(x)$) carrying a fraction "x" of the parent nucleon longitudinal momentum; x is a kinematic variable in DIS. We combine contributions from all partonic sub-processes that lead to the same final state and account for contributions that come from all possible x values by adding the partial cross sections.

The nucleon gluon distribution $xg(x)$ is known in the region $0.001 < x < 0.01$ (Fig. 2) but the nuclear distributions are not. Our present understanding of how parton distribution functions (PDFs) are changed when nucleons are bound in a nucleus is primarily derived from DIS of charged leptons from nuclear targets. The charged leptons used in DIS interact with the electrically charged quarks, not with the electrically neutral gluons, and provide measurements of structure functions, F_i. In the parton model, $F_2(x,Q^2) = x\sum_n e_n^2[q_n(x,Q^2) + \overline{q}_n(x,Q^2)]$, where e_n^2 is the squared electric charge of the quark of type n and Q^2 is the squared four momentum transfer of the scattered lepton, equated to the square of the scale at which the parton substructures are observed. Gluon densities are determined from the QCD evolution equations [17] applied to scaling violations of F_2 measured for the nucleon over an extremely large x and Q^2 range at the HERA collider [11,12]. Sensitivity to $g(x)$ in DIS is approximately given by the Q^2 variation of F_2 at half that x value, $g(2x) \propto \partial F_2(x,Q^2)/\partial(\ln Q^2)$ [18]. The kinematic range of the world data for the gluon distribution in nuclear targets is shown in the right panel of Fig. 2 as used in a recent global analysis of nuclear modifications to PDFs [6,7]. Such input to the nuclear gluon density is available only for $x > 0.02$ because nuclear DIS has been restricted to fixed target experiments. As will be discussed below, the study of d(p)+Au collisions at $\sqrt{s_{NN}}$=200 GeV can provide direct sensitivity to the nuclear modification of the gluon density for x values on the order of $x \sim 0.001$ and can test the universality of the nuclear gluon density in the range $0.02 < x < 0.1$. Comparable sensitivity in DIS to such low x would require an electron-ion collider [19]. Measuring the PDF with quark and gluon probes allows us to get to x and Q^2 values where saturation phenomena might be present.

3 Tests of parton saturation

Factorization theorems allow us to add cross sections rather than quantum amplitudes, with partons considered quantum mechanically independent of each another. Within this picture, we are tempted to imagine that the gluon distribution of a nucleus might be obtained by adding the gluon distributions for each nucleon, with some accounting for the relative motion of the nucleons in the nucleus. While perhaps true for large x processes, at small x the uncertainty principle tells us that the partons will all overlap in the longitudinal direction, so the partons do not interact independently. The front surface partons will interfere or shadow the back surface partons of the nucleus. For more than 20 years it has been recognized [20] that the quantum independence of partons cannot extend to very small x where the gluon density is very large.

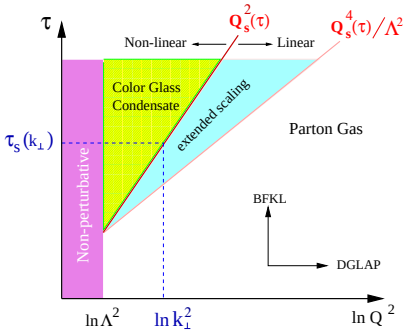

Fig. 3. Diagram showing the boundary between possible "phase" regions in the $\tau = \ln(1/x)$ versus $\ln(Q^2)$ plane [21]. BFKL evolution [22] results in expected exponential growth of the gluon density at fixed Q^2 and increasing τ. DGLAP evolution is discussed in the text.

To determine the scale at which collective behavior might become evident, the uncertainty principle suggests that a scattering process at fixed p_T will probe a transverse area approximately given by $S(p_T) = \pi(\hbar/p_T)^2$. For example at p_T = 2 GeV/c, this corresponds to about 0.3 mb, small in comparison to the proton cross sectional area of about 30 mb. The number of gluons that are present and that could shadow one another above x is nominally given by $n_{gluons}(x) = \int_x^1 g(x')dx'$. At x=0.01 $n_{gluons} \approx 7$, increasing by 7–8 for each order of magnitude decrease in the lower limit of x. At x=0.001, the product of cross section times number of gluons is $S(2\text{ GeV/c}) \times n_{gluons}(0.001) \approx$ 5 mb. This estimate suggests that for events with these kinematics, the chances of finding more than one gluon within the transverse resolution of the scattering probe is less than 20%. However in a nucleus of mass number A, the area of the nucleus grows roughly as $A^{2/3}$ while the number of gluons would nominally grow proportionally to A. Thus, the transverse density of nucleons should grow by a factor like $A^{1/3}$. For Au, this factor of 6 in transverse density suggests that shadowing could be substantial. By x=0.0001, it could become dominant. Of course, at lower p_T, the effects would show up at a larger value of x. Real predictions for the onset of shadowing vary with the model used [23], but whether shadowing modifies the gluon interactions at RHIC is an experimental question which must be answered with data.

For p+p collisions at $\sqrt{s}$=200 GeV, unlike at lower $\sqrt{s}$ [24], next-to-leading order (NLO) pQCD calculations [25] quantitatively describe inclusive particle production down to p_T of ~2 GeV/c using PDFs [4,5] and fragmentation functions [26,27] that describe the hadronization of the scattered partons. Furthermore, di-hadron azimuthal correlations have the same structure at these moderate p_T as they do at the highest possible p_T values, consistent with the idea that elastic scattering of quarks and gluons is responsible for the particle production [28].

Recent measurements at STAR using the prototype FPD already indicate that the factorized leading twist pQCD calculations work quite well to predict the $p+p \rightarrow \pi^0+X$ cross section in the $3 < \eta < 4$ region [10]. This gives

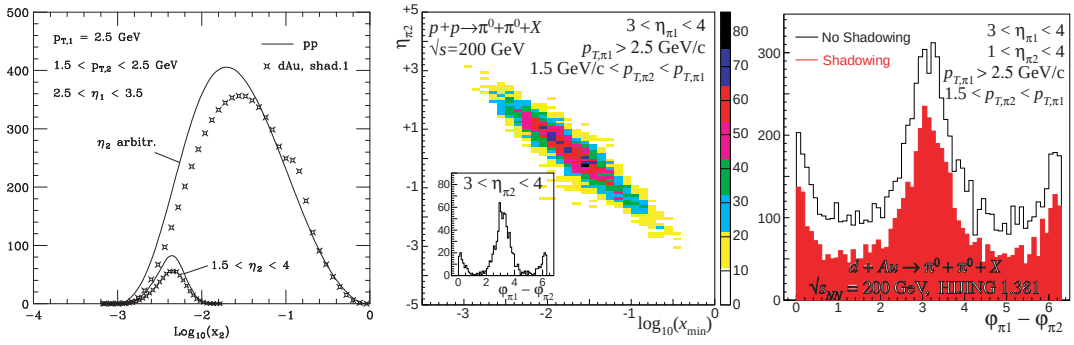

Fig. 4. (Left) pQCD calculation of $\pi^0 - \pi^0$ production at large η in p+p and d+Au collisions at $\sqrt{s_{NN}}$=200 GeV [33]. The distributions integrate to $d\sigma/dp_T$ in units of pb/GeV. The smallest x values are probed when $\pi^0 - \pi^0$ pairs are detected at large η. (Middle) PYTHIA [34] simulation for $\pi^0 - \pi^0$ production at large η in p+p collisions at $\sqrt{s}$=200 GeV. The η of the associated π^0 is strongly correlated with the x value of the soft parton involved in the partonic scattering. (Right) HIJING simulation for $\pi^0 - \pi^0$ production at large η in d+Au collisions at $\sqrt{s}$=200 GeV. Compared to the p+p simulations, the peaks in $\Delta\phi = \phi_{\pi 1} - \phi_{\pi 2}$ corresponding to elastic parton scattering, sit atop a background from other mechanisms for particle production.

confidence in the interpretation that at $\sqrt{s}$ =200 GeV the particle production process is dominated by leading twist quark- gluon scattering. With the FMS focusing on $\pi^0 - \pi^0$ pairs, we will select the low-x component shown by pQCD calculations (Fig. 4) to make only small contributions to the inclusive measurement. The low-x component of the forward pion yield is where shadowing effects are expected to be most important [29]. In the middle panel of Fig. 4 we see that when triggering on a π^0 in the range $3 < \eta < 4$, the rapidity of the second π^0 will reflect the x of the struck gluon. The right panel of Fig. 4 shows that elastic parton scattering is identified above physics backgrounds in d+Au collisions.

There has been considerable recent interest among the experts in the application of pQCD in reconciling the meaning of shadowing with the idea of universal (factorizable) PDFs. What has emerged recently [30] is a better understanding of just what the universal parton density means at small x. The present understanding is that the "shadowed" small x distributions should be universal but do not strictly reflect the probability for finding a parton. Included in the universal factorized functions are built-in final-state correlations with other gluons in the proton. We now see that even from the strict, leading twist perspective, low-x perturbation theory has a different interpretation from large x because it always involves a sampling of the macroscopic gluon fields. In light of this, there is real excitement that a variety of low-x phenomena from shadowing to large transverse spin asymmetries may be tied together with pQCD in ways not before appreciated.

Measurements of gluon shadowing at RHIC and the LHC will be essential input for models that predict the relationships between quark distributions and macroscopic gluon fields. Among the descriptions of shadowing or saturation effects is the Color Glass Condensate (CGC) [20, 31,32], an effective-field theory for understanding parton saturation. In the CGC picture, the saturation effects are associated with a new phase of the gluon field. The onset of this phase can be probed by measurements at small x and at small Q (related to the produced parton mass and the p_T associated with the scattering). Mapping out the boundaries (Fig. 3) for saturation signatures for back-to-back jet correlations as a function of x and p_T is a primary mission of the FMS.

4 Early results from RHIC

The first Au+Au collision runs at $\sqrt{s_{NN}}$=200 GeV resulted in the observation that high-p_T particle production at midrapidity was suppressed relative to expectations resulting from the scaling of yields from p+p collisions. The data also showed that two-particle correlations were suppressed when the particles were back-to-back (away-side, $\Delta\phi \approx 180°$) but not when they were fragments of the same jet (near-side,$\Delta\phi \approx 0$ or 2π) [36]. These observations are consistent with a prediction based on radiative energy loss of a high-p_T parton passing through a quark-gluon plasma [37]. A d+Au run at $\sqrt{s_{NN}}$ =200 GeV was scheduled early in the RHIC program to eliminate the possibility that this was due to initial state effects. For d+Au collisions, midrapidity particle production was found to have a small enhancement, consistent with the Cronin effect [38], and back-to-back correlations [39] more closely resembled results from p+p collisions than from Au+Au collisions. Hence, the suppression of back-to-back correlations in Au+Au collisions was attributed to the strongly interacting matter formed in those collisions, matter that was formed by interactions of the low-x gluons.

Measurements made by the BRAHMS collaboration for d+Au collisions [8] showed that inclusive particle production was suppressed as the rapidity of the observed particles increased. This provided a hint that the gluon distribution in the Au nucleus may be depleted at low-x. It is easy to understand how this suppression can occur within the standard pQCD picture of particle production. In that picture, the quarks and gluons each carry a fraction of their parent hadron momentum given by x. They elastically scatter and then fragment to the final state hadrons

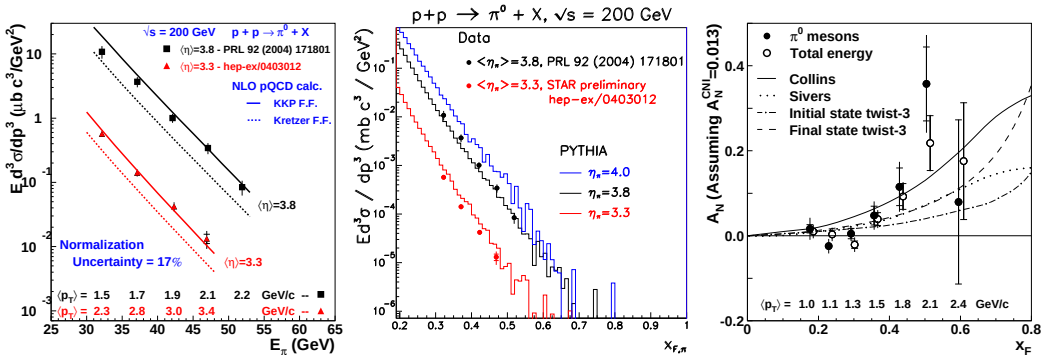

Fig. 5. (Left) Invariant cross sections for inclusive π^0 production at large rapidity in p+p collisions at $\sqrt{s}$=200 GeV [10,41] compared to NLO pQCD calculations [25,26,27]. (Middle) The data are compared with predictions from PYTHIA [34]. (Right) The analyzing power for π^0 production at $< \eta >$=3.8 in p+p collisions at $\sqrt{s}$=200 GeV [10]. The curves are predictions from pQCD models [46,48,50] evaluated at p_T=1.5 GeV/c.

observed with a given p_T and at a given η. For collinear parton pairs, it is easily shown that

$$x_+ \approx \frac{p_T}{\sqrt{s}}(e^{+\eta_1} + e^{+\eta_2}) \rightarrow x_F$$

$$x_- \approx \frac{p_T}{\sqrt{s}}(e^{-\eta_1} + e^{-\eta_2}) \rightarrow x_F e^{-(\eta_1+\eta_2)},$$

where the Feynman-x variable is $x_F = 2p_L/\sqrt{s}$, relevant in the limit $\eta_1 >> \eta_2$, and p_L is the longitudinal momentum component of the large η particle. For inclusive particle production, one of the two jets, or its hadronic surrogates, is observed at η_1 and the second jet has a broad η_2 distribution and $\Delta\phi \approx 180°$. By detecting a high energy hadron at large η_1, initial states with a large-x parton (most probably a quark) and a low-x parton (most probably a gluon) are selected. For each unit rapidity increase, the average x of the gluon from the initial state parent hadron is decreased by e. A similar decrease in x is a consequence of studying particle production in collisions at higher $\sqrt{s}$. Hence, the observed suppression of particle production at increasing rapidity can be interpreted as a reduction in the probability of finding gluons in the nucleus at small x.

The BRAHMS results [8] were confirmed in measurements by PHENIX [40]. The STAR collaboration also made measurements of large rapidity particle production and produced a limited data sample for two-particle correlations involving a large rapidity π^0 [28], measured with the FPD. The topology of the energy deposition in the FPD allows for robust measurements of the energy and direction of neutral pions. Since the π^0 is a pseudoscalar particle, kinematic distributions of its diphoton decay are exactly calculable in any frame of reference. Hence, calibrations of the FPD response can be obtained at the level of ∼1% simply by requiring a fully consistent response of all cells of the calorimeter to the photons produced by the $\pi^0 \rightarrow \gamma\gamma$ decay. This same technique will be used for the FMS. Figure 5 also shows that the simulation code PYTHIA [34] is able to reproduce the absolute cross section of the produced π^0 from p+p collisions. In addition, nearly all features of the $\Delta\phi$ distributions for charged hadrons with $|\eta| < 0.75$ coincident with forward π^0 are reproduced by PYTHIA. This gives us a tool to guide the design of the FMS and the interpretation of the data.

5 Proton spin with the FMS

Our understanding of the two-particle correlations involving large rapidity particles, and our ability to use these correlations to measure nuclear gluon distributions, is a direct result of the methodology developed to understand the first spin asymmetry measurements at RHIC. It is no surprise that the FMS will also be a powerful tool in studying the spin structure of the proton.

An early prediction of pQCD was that, at leading twist and with collinear factorization, the chiral properties of the theory would make the analyzing power(A_N) small for particles produced with transversely polarized proton beams [42]. A_N is derived from the azimuthal asymmetry of particle yields from a transversely polarized beam incident on an unpolarized target. However, from AGS energies [43] to Fermi Lab energies [44] and most recently at STAR [10] (Fig. 5), a large transverse single spin asymmetry has been observed. The consistent trend is that A_N in $p_\uparrow + p \rightarrow \pi^0 + X$ increases rapidly for x_F above about 0.3. Transverse single spin asymmetries have also been observed in semi-inclusive DIS from polarized targets [45] and experimental studies of these spin effects is an active area of research. The FMS is ideally suited to extend these studies. Calculations of twist-3 contributions [46] to the observed A_N provide terms that may be related to macroscopic gluon fields in the polarized nucleon.

There are multiple phenomenological effects that have been identified as possible sources for the large A_N, but only two that are expected to be large. One is the Sivers effect [47,48], which is an initial state correlation between the parton intrinsic transverse momentum k_T and the transverse spin of the nucleon, $A_N \propto \boldsymbol{S}_T \cdot (\boldsymbol{P} \times \boldsymbol{k}_T)$, where $\boldsymbol{P}$ is the beam momentum and $\boldsymbol{S}_T$ is the transverse proton spin. In the Sivers framework, A_N is sensitive to the contribution of quark orbital angular momentum to the

nucleon spin. Large A_N is the result of a spin dependent p_T trigger bias favoring events where k_T is in the same direction as p_T.

If the Sivers effect is present, we can further characterize it with a measurement of the away side jet. The k_T of the initial-state parton can be measured when final-state jet pairs are not exactly back to back ($\Delta\phi = 180°$) [55]. The spin dependence of this k_T measurement is exactly what the Sivers model predicts.

While the Sivers effect connects A_N to the orbital angular momentum of quarks, a second effect, called the Collins effect [49,50], is directly sensitive to the transversity distribution function [51,52], related to the transverse polarization of quarks (and antiquarks) in a transversly polarized proton [53]. Here the quark scatters, preserving its transverse spin, and then fragments into pions and other hadrons. The fragmentation function reveals the polarization of the fragmenting quark and thus the initial quark state. In this example, the asymmetry does not appear in the jet production directly, but only in the fragmentation. The jet axis would not show the transverse asymmetry, but a pion fragment would. Recent calculations that include the full k_T dependence in the convolution integrals provide some indication that the Collins effect may be small [54].

The FMS will be able to distinguish between these mechanisms. By looking at pairs of same-side neutral pions, we can measure A_N as a function of the two pion kinematics. With the FMS we will separately measure the contributions to A_N that comes from the jet axis versus that which comes from the jet structure. Many theory papers have studied this problem: however, the need for data is great. The FMS STAR experiments on transverse polarization will provide to theorists the necessary input to determine the relative contributions from the Sivers effect and the Collins effect.

6 FMS Configuration

The STAR FPD now taking data acts as the prototype for the proposed FMS. Our results with the FPD demonstrate the feasibility of large rapidity measurements with electromagnetic calorimetry in both p+p and d+Au collisions at $\sqrt{s_{NN}}$=200 GeV at RHIC. Each FPD calorimeter is a 7×7 matrix of 3.8cm $\times$ 3.8cm $\times$ 45cm lead-glass cells that can be positioned in the range $3.3 < \eta < 4.0$. These are identical to the 684 small cells to be used in the FMS and the techniques we have developed for FPD tuning and analysis are directly applicable to the FMS. By implementing the FMS in STAR, the study of $\gamma - \pi^0$ and $\pi^0 - \pi^0$ correlations in both rapidity and azimuthal angles is enabled over $-1 < \eta < 4$. The FMS also allows inclusive measurements of π^0, γ and the production of heavy mesons that decay to all γ final states over a broad range of η and p_T. A schematic of the proposed FMS detector is shown in Fig. 6, along with examples of the mass resolution from a topological analysis [56] of the energy deposition for data obtained with the current FPD. We expect to achieve 1% accuracy in the calibration of the

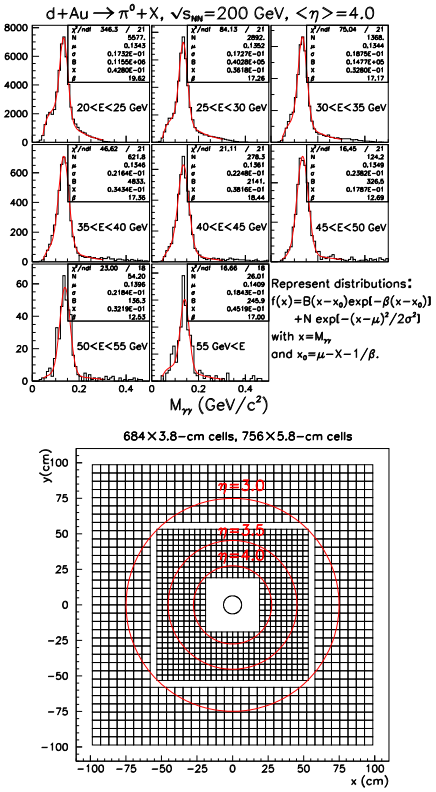

Fig. 6. (Top) Di-photon invariant mass distributions from the STAR FPD for d+Au collisions at $\sqrt{s_{NN}}$=200 GeV at $< \eta >$=4.0 relative to the incident deuteron beam. (Bottom) Layout of the proposed FMS.

FMS, just as we have done for the FPD. Energy resolution of $< 15\%/\sqrt{E}$ has been demonstrated. Simulation studies compare well to FPD data and show that we can expect to locate the π^0 to better than 0.5 cm (RMS). Our expected π^0 mass resolution is $\sim$23 MeV/c^2 based on experience with the FPD. For neutral pions with $20 < E < 60$ GeV the reconstruction efficiency of the FPD is just given by geometry. To predict event yields, we used a very conservative estimate of 35% for reconstruction and geometric efficiency. The FMS will provide complete azimuthal coverage for the pseudorapidity interval $2.5 < \eta < 4.0$ and will be built from existing lead-glass cells.

7 Plan for measurements

We will concentrate on measurements directed at our three immediate physics goals for d+Au and for p+p running. In a future d+Au run at $\sqrt{s}$=200 GeV we will determine the gluon distribution in the gold nucleus. The large acceptance of the FMS will provide good statistics for comparisons of identified π^0 yields in p+p and d+Au collisions over a very broad range in p_T and pseudorapidity. We will measure the correlations between a trigger particle in the FMS (either a π^0 or a γ) and a second particle (jet surrogate) in the TPC, BEMC, EEMC or FMS. The

threshold p_T for the trigger and coincident particles will be investigated over the range from $1 < p_T < 4$ GeV/c. The large size and high granularity of the FMS allow us to identify neutral pions at energies down to ∼10 GeV, where hadronic energy deposition becomes a significant background. At maximum rapidity, this determines our lowest observable p_T threshold. As seen in Fig. 4, the η of the coincident particle correlates with the gluon x value. The $\Delta\phi$ distribution reveals the scattering history. To develop the full picture of the gluon distributions, we will investigate the dependence of $\pi^0 - \pi^0$ correlations on Q^2. To determine the dynamical origin (Sivers or Collins) of the observed transverse single spin asymmetry for forward π^0 production, we will make similar correlation measurements in the polarized p+p run.

As shown in Fig. 4, pQCD calculations [33] suggest that the lowest x values for the gluon density are probed when both jets from the elastic parton scattering are produced at large rapidity. Both $\pi^0 + \pi^0$ and $\pi^0 + \gamma$ final states can be analyzed in the FMS. The p_T of the π^0 must be large enough to favor elastic parton scattering over inelastic scattering [28] although both contributions are contained in PYTHIA and NLO pQCD calculations. The large size of the proposed FMS enables the use of isolation cuts to distinguish between π^0 decay photons and direct photons. The dominant subprocess for direct photon production at RHIC is QCD Compton scattering, $qg \rightarrow \gamma q$. This can also be used to probe the small x gluon density with only minimal physics backgrounds.

Figure 4 shows a HIJING 1.381 [35] simulation of 7.5×10^8 minimum-bias d+Au events at $\sqrt{s_{NN}}$=200 GeV, from which all $\pi^0 - \pi^0$ pairs with the specified p_T and η are selected and used to compute $\Delta\phi$. Unlike the case for p+p collisions, the elastic parton scattering peaks in the $\Delta\phi$ distribution sit atop a background from the nuclear collision. Despite the background, the elastic parton scattering is readily discriminated and can be identified as the expected peak in $\Delta\phi$. We can quantitatively describe these distributions from $1 < \Delta\phi < 5.28$ radians by a Gaussian function, used to model the peak, and a constant background. A best fit to the $\Delta\phi$ distribution in Fig. 4 results in 2.3×10^3 events in the peak for simulations done without shadowing and $\sim 1.8 \times 10^3$ events in the peak for the simulations done with shadowing. We can expect that a 10-week d+Au run will allow us to sample $> 6 \times 10^{10}$ minimum-bias interactions, based on RHIC performance for d+Au collisions achieved in the last weeks of run 3. Accounting for detector efficiencies for the FMS and endcap EMC, the simulations suggest we will observe at least 8×10^3 events in the $\Delta\phi$ peak without shadowing. This is enough to investigate the spatial dependence of the nuclear gluon density [13,14] using particle multiplicity measurements in the Au beam direction made by other STAR subsystems to determine sensitivity to the impact parameter of the collision. Broadening or disappearance of the away-side correlation could signal the transition to a macroscopic gluon field at sufficiently low x.

For the polarized proton running, we base estimates of the rate of near-side $\pi^0 - \pi^0$ pairs on PYTHIA [34]. The STAR measurements (Fig. 5) show that A_N is small below $x_F \sim 0.4$, and increases monotonically as x_F of the forward π^0 increases. In the Sivers picture, A_N should be associated with the forward jet and should be present for $\pi^0 - \pi^0$ pairs from the same jet. We would expect a large A_N when $x_{F1} + x_{F2} > 0.4$. When one π^0 is observed at $3 < \eta < 4$ with $x_{F1} > 0.25$ and a second π^0 is observed with $\eta < 4$ and $x_{F2} > 0.15$ and the $\pi^0 - \pi^0$ pair has $|\eta_1 - \eta_2| < 0.5$, the simulated $\Delta\phi$ correlation shows a jet-like near-side correlation peak sitting atop a uniform background attributed to the underlying event. We expect $\sim 1.5 \times 10^4$ $\pi^0 - \pi^0$ events in the near-side jet-like peak for 1 pb^{-1} of integrated luminosity for polarized p+p collisions at $\sqrt{s} = 200$ GeV with the FMS. For a beam polarization of 50% this would result in a statistical error on the analyzing power of $\delta A_N \sim 0.01$. The Collins mechanism attributes A_N to the correlation between the momenta of two hadrons from the same jet and the proton spin vector. The transverse momentum associated with jet fragmentation producing a π^0 with $x_{F1} > 0.4$ and $3 < \eta < 4$ can be measured by detecting a second π^0 with $\eta < 4$ and $x_{F2} > 0.15$ and requiring the $\pi^0 - \pi^0$ pair have $|\eta_1 - \eta_2| < 0.5$. Again, the $\Delta\phi$ correlation shows a jet-like near-side correlation peak sitting atop a uniform background. For these kinematics, we expect 2×10^3 $\pi^0 - \pi^0$ pairs in the jet-like near-side $\Delta\phi$ peak for 1pb^{-1} of integrated luminosity. If a non-zero Collins effect is observed, then larger integrated luminosity samples would be required to map out the x dependence of the transversity structure function.

8 Summary

Early experimental results from RHIC, coupled with theoretical developments that demonstrate the robustness of NLO pQCD calculations at collider energies down to moderate p_T values, suggest that a quantitative determination of the gluon density in a heavy nucleus can be obtained at an order of magnitude lower x than available from DIS on nuclear targets. Such studies require improved instrumentation in the forward direction at RHIC. In addition to providing crucial information to understand the initial state of heavy-ion collisions that may lead to a quark-gluon plasma, future low-x studies at RHIC may establish the existence of a macroscopic gluon field. Improved forward instrumentation can also disentangle the dynamical origin of transverse single spin asymmetries.

References

1. "*Experimental and Theoretical Challenges in the Search for the Quark Gluon Plasma*" (STAR collaboration) [nucl-ex/0501009]; "*Formation of dense partonic matter in relativistic nucleus-nucleus collisions at RHIC*" (PHENIX collaboration), [nucl-ex/0410003]; "*Quark Gluon Plasma and Color Glass Condensate at RHIC?*" (BRAHMS collaboration), [nucl-ex/0410020]; "*The PHOBOS Perspective on Discoveries at RHIC*" (PHOBOS collaboration), [nucl-ex/0410022].

2. Miklos Gyulassy and Larry McLerran, RBRC Scientific Articles Vol. 9 [nucl-th/0405012].
3. Peter D. Barnes *et al.* "*U.S. Program in Heavy-Ion Nuclear Physics: Scientific Opportunities and Resource Requirements*", October, 2004 (unpublished).
4. J. Pumplin, D.R. Stump, J. Huston, H.L. Lai, P. Nadolsky, W.K Tung, JHEP **0207** (2002) 012.
5. A.D. Martin, R.G. Roberts, W.J. Stirling, R.S. Thorne, Eur. Phys. J **C28** (2003) 455.
6. M. Hirai, S. Kumano, T.-H. Nagai, Phys. Rev. **C70** (2004) 044905.
7. "*PDFs, Shadowing and pA Collision*", CERN Yellow Report on Hard Probes in Heavy Ion Collisions at the LHC (HIP-2003-40/TH), K.J. Eskola (editor) [hep-ph/0308248]; and K.J. Eskola, H. Honkanen, V.J. Kolhinen and C.A. Salgado [hep-ph/0302170].
8. I. Arsene *et al.* (BRAHMS collaboration), Phys. Rev. Lett. **93** (2004) 242303.
9. K.H. Ackermann *et al.*(STAR collaboration), Nucl. Instrum. Meth. **A499** (2003) 624.
10. J. Adams *et al.* (STAR collaboration), Phys. Rev. Lett. **92** (2004) 171801 [hep-ex/0310058].
11. C.Adloff *et al.* (H1 Collaboration), Eur. Phys. J. **C21** (2001) 33 [hep-ex/0012053]. I. Abt *et al.* (H1 collaboration), Nucl. Phys. **B407** (1993) 515.
12. S. Dhekanov *et al.* (ZEUS Collaboration), Eur. Phys. J. **C21** (2001) 443 [hep-ex/0105090]. M. Derrick *et al.* (ZEUS collaboration), Phys. Lett. **B316** (1993) 412.
13. L. Frankfurt, M. Strikman, S. Liuti, 4^{th} RHIC Workshop on Experiments and Detectors (1990) 103.
14. V. Emel'yanov, A. Khodinov, S.R. Klein, R. Vogt, Phys. Rev. **C61** (2000) 044904.
15. Jianwei Qiu, Ivan Vitev, Phys. Rev. Lett. **93** (2004) 262301.
16. D. Kharzeev, E. Levin, L. McLerran (to be published) [hep-ph/0403271].
17. Yu.L. Dokshitzer, Sov. Phys. JETP **46** (1977) 641; V.N. Gribov, L.N. Lipatov, Sov. Journ. Nucl. Phys. **15** (1972) 438 and 675; G. Alttarelli, G. Parisi, Nucl. Phys. **B126** (1977) 298.
18. K. Prytz, Phys. Lett. **B311** (1993) 286.
19. A. Deshpande, R. Milner, R. Venugopalan, *The Electron Ion Collider*, BNL report 68933 (2002).
20. L.V. Gribov, E.M. Levin, M.G. Ryskin, Phys. Rept. **100** (1983) 1.
21. Edmond Iancu, Raju Venugopalan, Quark Gluon Plasma 3, R.C. Hwa and X.-N. Wang (eds.), World Scientific, 2003 [hep-ph/0303204].
22. L.N. Lipatov, Sov. J. Nucl. Phys. **23** (1976) 338; E.A. Kuraev, L.N. Lipatov, V.S. Fadin, Sov. Phys. JETP **45** (1977) 199; Ya.Ya. Balitsky, L.N. Lipatov, Sov. J. Nucl. Phys. **28** (1978) 822.
23. Leonid Frankfurt, Vadim Guzey, Mark Strikman, J. Phys. **G27** (2001) R23 [hep-ph/0010248].
24. C. Bourrely, J. Soffer, Eur. Phys. J. **C36** (2004) 371 [hep-ph/0311110].
25. F. Aversa *et al.*, Nucl Phys. **B327** (1989) 105; B. Jager *et al.*, Phys. Rev. **D67** (2003) 054005; and D. de Florian, Phys. Rev. **D67** (2003) 054004.
26. B.A. Kniehl, G. Kramer, B. Poetter, Nucl Phys. **B597** (2001) 337.
27. S. Kretzer, Phys. Rev. **D62** (2000) 054001.
28. A. Ogawa (for the STAR collaboration), contribution to DIS2004 [hep-ex/0408004].
29. R. Vogt, Phys. Rev. C (in press) [hep-ph/0405060].
30. S. Brodsky, P. Hoyer, N. Marchal, S. Peigne, F. Sannino, Phys. Rev. **D65** (2002) 114025.
31. A.H. Mueller, J. Qiu, Nucl. Phys. **B268** (1986) 427; J.-P. Blaizot, A.H. Mueller, Nucl. Phys. **B289** (1987) 847.
32. L.D. McLerran, R. Venugopalan, Phys. Rev. **D49** (1994) 2233; (1994) 3352; **D50** (1994) 2225.
33. V. Guzey, M. Strikman, W. Vogelsang, Phys. Lett. **B603** (2004) 173 [hep-ph/0407201].
34. T. Sjöstrand, P. Eden, C. Friberg, L. Lönnblad, G. Miu, S. Mrenna, E. Norrbin, Computer Physics Commun. **135** (2001) 238.
35. X. N. Wang, M. Gyulassy, Phys. Rev. **D44** (1991) 3501.
36. C. Adler *et al.* (STAR collaboration), Phys. Rev. Lett. **90** (2003) 082302.
37. M. Gyulassy, M. Plümer, Phys. Lett. **B243** (1990) 432; X.N. Wang, M. Gyulassy, Phys. Rev. Lett. **68** (1992) 1480.
38. D. Antreaysan *et al.*, Phys. Rev. **D19** (1979) 764.
39. J. Adams *et al.* (STAR collaboration), Phys. Rev. Lett. **91** (2003) 072304.
40. S.S. Adler *et al.* (PHENIX collaboration), submitted to Phys. Rev. Lett. [nucl-ex/0411054].
41. L.C. Bland (for the STAR collaboration) contribution to 10^{th} Workshop on High Energy Spin Physics (Dubna, 2003) [hep-ex/0403012].
42. G.L. Kane, J. Pumplin, W. Repko, Phys. Rev. Lett. **41** (1978) 1689.
43. R.D. Klem *et al.*, Phys. Rev. Lett. **36** (1976) 929; W.H. Dragoset *et al.*, Phys. Rev. **D18** (1978) 3939; S. Saroff *et al.*, Phys. Rev. Lett. **64** (1990) 995; B.E. Bonner *et al.*, Phys. Rev. **D41** (1990) 13; K. Krueger *et al*, Phys. Lett. **B459** (1999); C.E. Allgower *et al.*, Phys. Rev. **D65** (2002) 092008.
44. B.E. Bonner *et al.* Phys. Rev. Lett. **61** (1988) 1918; D.L. Adams *et al.*, Phys. Lett. **B261** (1991) 201; Phys. Lett. **B264** (1991) 462; Z. Phys. **C56** (1992) 181; A. Bravar *et al.* Phys. Rev. Lett. **77** (1996) 2626.
45. A. Airapetian *et al.* (HERMES), Phys. Rev. Lett. **94** (2005) 012002.
46. A. Efremov, O. Teryaev, Phys. Lett. **B150** (1985) 383; J. Qiu, G. Sterman, Phys. Rev. **D59** (1998) 014004; Y. Koike, AIP Conf. Proc. **675** (2003) 449.
47. D.Sivers, Phys. Rev. **D41** (1990) 83; 43 (1991) 261.
48. M. Anselmino, M. Boglione, F. Murgia, Phys. Lett. **B362** (1995) 164; M. Anselmino, F. Murgia, Phys. Lett. **B442** (1998) 470.
49. J. Collins, Nucl. Phys. **B396** (1993) 161; J. Collins, S.F. Heppelmann, G.A. Ladinsky, Nucl. Phys. **B420** (1994) 565.
50. M. Anselmino, M. Boglione, F. Murgia, Phys. Rev. **D60** (1999) 054027.
51. J.P. Ralston, D.E. Soper, Nucl. Phys. **B152** (1979) 109.
52. R.L. Jaffee, X.D. Ji, Phys. Rev. Lett. **67** (1991) 552.
53. V. Barone, A. Drago, P.G. Ratcliffe, Phys. Rept. **359** (2002) 1.
54. M. Anselmino, M. Boglione, U. D'Alesio, E. Leader, F. Murgia, contribution to SPIN2004 [hep-ph/0412236]; M. Anselmino, M. Boglione, U. D'Alesio, E. Leader, F. Murgia, (to be published) [hep-ph/0408356].
55. Daniel Boer, Werner Vogelsang, Phys. Rev. **D69** (2004) 094025 [hep-ph/0312320].
56. A.A. Lednev, Nucl. Instrum. Meth. **A366** (1995) 292.